

f -mode Imprints in Gravitational Waves from Coalescing Binaries Involving Spinning Neutron Stars

Hao-Jui Kuan^{1,2,*} and Kostas D. Kokkotas¹

¹*Theoretical Astrophysics, IAAT, University of Tübingen, Tübingen, D-72076, Germany*

²*Department of Physics, National Tsing Hua University, Hsinchu 300, Taiwan*

(Dated: Thursday 5th May, 2022)

The excitation of f -mode in a neutron star member of coalescing binaries accelerates the merger course, and thereby introduces a phase shift in the gravitational waveform. Emphasising on the tidal phase shift by rotating stars, we provide an accurate, yet economical, method to generate f -mode-involved, pre-merger waveforms using realistic spin-modulated f -mode frequencies for some viable equations of state. We find for slow-rotating stars that the dephasing effects of the dynamical tides can be uniquely, EOS-independently determined by the direct observables (chirp mass \mathcal{M} , symmetric ratio η and the mutual tidal deformability $\tilde{\Lambda}$), while this universality is gradually lost for increasing spin. Although a high cutoff waveform frequency combined with large signal-to-noise ratio (SNR) is needed to trace the tidal dephasing if binary members rotate slowly, for binaries with fast rotating members ($\lesssim 800$ Hz) the phase shift due to f -mode will exceed the uncertainty in the waveform phase at reasonable SNR ($\rho = 25$) and cutoff frequency of $\gtrsim 400$ Hz. In addition, a significant phase shift of $\gtrsim 100$ rads can be found for a high cutoff frequency of 10^3 Hz. For systems involving a rapidly-spinning star (potentially the secondary of GW190814), neglecting f -mode effect in the waveform templates can therefore lead to considerable systemic errors in the relevant analysis.

I. INTRODUCTION

A. The Context

The macroscopic and microscopic properties of neutron stars (NSs) in coalescing binaries are imprinted in the emitted gravitational waveforms. The precise knowledge of the waveform morphology is of fundamental importance in the signal analysis and the extraction of the NS parameters therefore. Adopting the point-particle approximation for the gravitational wave (GW) analysis, the chirp mass and the symmetric mass of binaries can be estimated from the 1st order post-Newtonian (PN) phase evolution of GWs, though with different degree of accuracy [1–6]. Beyond the point-particle baseline approximants, the internal structure of the NS members can also be probed: the quadrupole deformations induced by the tidal forces in the constituents will affect the binary evolution and thus the associated waveform. Two sorts of (gravito-electric) tidal effects are involved in the signal, viz. the equilibrium tides due to the induced tidal deformations, and dynamical tides due to the resonant excitation of the various neutron star quasi-normal modes (QNMs). Equilibrium tidal effects from Newtonian [5, 7], 1 PN [8, 9], up to 2.5 PN level [6], are encapsulated in the tidal deformability, and their traces in the signal have already been observed with the current detectors (see [10] and [11] for a recent review). Dynamical tides, while being subdominant in the low frequency regime, can affect the waveform to a similar extent as the equilibrium ones at the final stage of inspiraling, predominantly due to the f -mode excitation [12–15].

For rotating NS progenitors, the spin-effects also contribute to phase shift thus introducing some degeneracy with the tidal contributions (cf. Eq. (3) of [16]). For instance, the spin-orbit (comes at 1.5 PN order), and the secondary spin-spin (comes at 2 PN order) terms appear in the PN expression of GW phase [17–19]. In addition, rotation will induce a quadrupole deformation on the star, and its gravitational potential would be deformed accordingly. The deformation is larger for stiffer EOS [20] since NSs tend to have larger radius [21]. The change in the gravitational potential modifies the relation between the angular velocity and the separation of stars. The binary motion is affected by this self-spin effect at the same level as spin-spin effect (i.e., 2 PN) [22, 23], whose contribution to GW dephasing is however much smaller than the tidal one (see, e.g., Fig. 4 of [24]).

Rotation introduces shifting and splitting of the QNM spectrum of NSs, and thereby alters the tidal effects and as a consequence the waveform [25]. The effect of stellar rotation in the tidal dephasing is more profound for increasing spin rate since the downward-tuned QNM frequencies (counter rotating) lead to stronger tidal excitations. Although there are higher order couplings between tides and rotation, e.g., tide-spin terms, these are considerably weaker than the aforementioned effects, and even the accuracy of the state-of-the-art numerical relativity (NR) is incapable of sizing these effects [16]. Owing to the interplay between spin and tides, the ambiguity in the spins of inspiralling NSs would consequently obscure the determination of tidal dephasing especially if one of the NSs spins rapidly (e.g., [26, 27]). For the precise extraction of the source properties, it is thus important to discriminate tidal dephasing from the phase shift generated due to spin-contributions.

In addition to the degeneracy of spin and tidal dephasing, the uncertainty in equation of state (EOS) further

* hao-jui.kuan@uni-tuebingen.de

messes up the attribution of the phase shifts to individual effects without knowing the “correct” EOS *a priori* (e.g., [28]); currently, several candidates survive the observations of pulsars [29, 30], and GW170817 as well as its electromagnetic counterparts [10, 31, 32]. Nonetheless, the f -mode effects in dephasing may overcome the uncertainty in phase originating from the EOS in some circumstances [33], where a neat clue of dynamical tidal effects can be observed. In a pursue of reliable analysis, it is necessary to take f -mode effect into account when constructing gravitational waveform templates for those cases [33–35].

The tidal effects of rotating NSs in binaries have been investigated in [25] by adopting an approximation for the frequency modulations [see Eq. (5.7) therein], which engulf a variance of $\lesssim 15\%$ among the realistic values (cf. Fig. 10 in [36]). In the present article, we re-examine the measurability of dynamical tidal dephasing by using the realistic spin-modulation in the QNM spectrum, and a PN evolution for the inspiral part.

B. This Work

On top of a great body of existing literature, we collate in the following the original contribution of this article to address f -mode effect in GW:

- *EOS-independent Hamiltonian* — For slow-rotating binary NSs, the Hamiltonian of the binary evolution, including the tidal effects, is shown to be EOS-independently reconstructable from GW observable \mathcal{M} , η , and $\tilde{\Lambda}$ [Eq. (26)] since f -mode effects can be prescribed universally by Λ_\star [Eqs. (23)–(25)]. Assuming we have a well-measured chirp mass [2, 4, 37], say $\mathcal{M} = 1.146$ (the value for GW170817 [38]), the accumulated GW phase Ψ_{tot} is shown to be a universal function of the mass of the primary M_\star (Fig. 4).

- *“Observability” of the spin effects in tidal dephasing* — Adopting five EOS with some representative spin rates, we find that the tidal dephasing piles up rapidly at the high frequency regime of GW (top panel of Fig. 5), hinting at that the information of dynamical tides concentrates in this part of waveform. On the other hand, the accumulated tidal dephasing from 20–1000 Hz of f_{gw} is larger for higher stellar spins for stiffer EOS (bottom panel of Fig. 5). For the highest stiffness EOS considered, viz. MPA1, we find a few tens rad of dephasing if two stars rotate moderately, while a few hundreds rad can be achieved when stars rotates rapidly. Although we consider symmetric binaries (masses and spins of both stars are the same) for Fig. 5, the conclusion is expected to be general since (i) faster rotation leads to further frequency reduction which will enhance the tidal dephasing, and (ii) NSs with stiffer EOS tend to have larger radii thus more notable tidal deformations. Despite of its dependence on EOS, the tidal dephasing can be expressed as a universal relation with respect to a dimensionless spin [Fig. 6; Eq. (29)].

- *Fast-spinning NS* — In general, the SNR needed to measure the tidal dephasing $\Delta\Psi^T$ depends on the cut-off frequency of the data stream f_{max} , as well as the spin of the primary $\Omega_{\text{s},\star} = 2\pi\nu_{\text{s},\star}$. As an example, we assume a specific binary and trace that the error in GW phase decreases for increasing f_{max} , while the tidal dephasing increases for larger f_{max} (top panel of Fig. 7). In this case, a data stream continuing beyond 600 Hz suffices to make the accumulated tidal dephasing exceed the uncertainty in the GW phase. Additionally, we see that a considerable improvement, in the measurability of tidal dephasing, can be made even by extending the cutoff frequency from 400 Hz to 500 Hz if the primary has a moderate spin ($\lesssim 400$ Hz). Although the improvement for rapidly-spinning primary by extending f_{max} is weaker (bottom panel of Fig. 7), the required SNR for such system is much lower anyway; a mild SNR of $\rho \lesssim 20$ is sufficient to discriminate the tidal dephasing even for a cutoff $f_{\text{max}} = 400$ Hz if the secondary of GW190814 is a fast-rotating NS with $\nu_{\text{s},\star} > 800$ Hz. *The sizable f -mode effects quantified in the present article indicate that templates including f -mode effects are imperative for inferring EOS from more accurate GW observation in the near future.* That said, if a rapidly-rotating NS is involved in a coalescing binary, as it is claimed for the secondary of GW190814 [39–41], the f -mode effects enhanced by the fast rotation will be unambiguously measurable in the signal. Neglecting f -mode effects in such events will therefore result in biased inferences of stellar parameters.

The article is organised as following: We summarise the present status of the analytical waveform derived from the effective-one-body approach in Sec. II. Tidal dephasing is numerically studied in Sec. III, where the dependence on EOS, and the tidal effects of spinning NS are detailed. In addition, we illustrate how to discriminate tidal effects from spin-orbit effects. A particular investigation on the influence in the GW phase produced by the spin-modified f -mode excitation is applied to GW190814 in Sec. IV. Finally, a discussion of the results is included in Sec. V.

Unless stated otherwise, all quantities are given in the unit of $c = 1 = G$.

II. TIDAL DEPHASING: ANALYTIC MODELS

Under the stationary phase approximation (SPA) and by ignoring the PN modifications in the GW amplitude \mathcal{A}^1 , the frequency-domain gravitational waveform can be

¹ In general, the amplitude $\mathcal{A}(f_{\text{gw}})$ depends on the internal structure (or finite size effects) of the binary members, the omission of these higher PN corrections does not affect the accuracy of SPA. In practice, SPA will be quite accurate up to the merger [6, 42], and thus this approximation will not affect significantly our results.

expressed by: [3, 4]

$$h(f_{\text{gw}}) = \mathcal{A} f_{\text{gw}}^{-7/6} e^{i\Psi(f_{\text{gw}})}. \quad (1)$$

This form is generic for all kinds of compact binaries. Here, $f_{\text{gw}} = \Omega_{\text{orb}}/\pi$ is the GW frequency, and Ω_{orb} is the orbital frequency. The phase $\Psi(f_{\text{gw}})$ is related to the time domain phase $\phi(t)$ via

$$\Psi(f_{\text{gw}}) = 2\pi f_{\text{gw}} t_o - \phi(t_o) - \frac{\pi}{4}, \quad (2)$$

and obeys the equation [6, 15, 43]

$$\frac{d^2\Psi}{d\Omega_{\text{orb}}^2} = \frac{2Q_\omega}{\Omega_{\text{orb}}^2}, \quad (3)$$

where t_o is a reference time with $\phi_o = \phi(t_o)$ being the corresponding phase, and Q_ω is a dimensionless measure of the phase acceleration defined as

$$Q_\omega = \Omega_{\text{orb}}^2 \left(\frac{d\Omega_{\text{orb}}}{dt} \right)^{-1}. \quad (4)$$

Constructing precise waveforms demands an accurate evolution of coalescing binaries. The PN equations of motion describe with adequate accuracy the largest part of the observed inspiralling evolution [44]. Still the PN approximation gradually fails as the binary approaches the plunge, merger, and finally the ringdown phases. This lack of applicability for high orbital frequencies and the post-merger dynamics motivated the so-called effective-one-body (EOB) formalism, which re-sums the PN expansions to account properly for the higher-order effects [45, 46]. In addition, the EOB analytic dephasing can be “calibrated” with the late-time NR results [47] even when tidal effects are taken into account [48, 49]. However, the latter hybrid EOB and NR model is much more time-consuming than the PN formalism. In the present article, we are not to study the tidal influence on high frequency waveform, but aim to offer an economical waveform variant capable to probe the internal physics of NSs from the low-frequency part of the waveform (before the actual “merger” begins; $\lesssim 10^3$ Hz). To this end, the PN framework proves sufficiently accurate [50–52] (see also below).

Tidal interactions among the binary members (i) accelerate the shrinking rate due to orbital energy transfer to QNMs [12, 53], or, in another perspective, effectively amplify the strength of the gravitational potential in the EOB framework [52, 54, 55], (ii) enhance the energy flux carried by GW due to tidal deformations (see, e.g., Eq. (3.6) of [8]), and (iii) increase the angular momentum loss. As a result, certain tidally-driven modifications in \mathcal{A} and Ψ will be encoded, while the change in \mathcal{A} is minor.

The effect of equilibrium tides in the phase shift is mainly governed by the quadrupolar tidal deformability

of the NSs in the binary [5, 7],

$$\Lambda = \frac{2k_2}{3C^5} \quad (5)$$

where k_2 is the (dimensionless, quadrupolar) tidal Love number, and $C = M/R$ is the stellar compactness. The contribution of the higher-order Love numbers in the phase-shift is significantly smaller [16]. On the other hand, the dynamical tides are resulted from the excitation of oscillations in the individual NSs, which are predominantly excited by the quadrupolar ($l = 2$) component of the tidal potential built by the companion (see, e.g., the discussion in the Appendix A.2 of [6]). Among the various low or high frequency modes (p -, g -, i -, w -, etc.), the contribution of the f -mode is more significant to the tidal response, strictly the $l = 2 = m$ f -mode [6, 12, 16, 56]. Therefore, we restrict ourselves to the physics (f -mode, tidal potential and deformability) at the quadrupolar level to study the leading order tidal phenomena. Although we focus on the quadrupolar f -mode, our methodology is applicable to higher-order ($l > 2$) f -modes and to other types of modes.

On top of the tidal interaction, the spins of the constituents also influence the binary evolution via spin-orbit, self-spin couplings [17, 18, 57, 58], and some higher order terms such as spin-tidal coupling. Incorporating the aforementioned physics, and by denoting a certain parameter X of the primary (companion) as X_\star (X_{comp}), the GW phase can be expressed as

$$\Psi = \Psi(f_{\text{gw}}; \mathcal{T}, \mathcal{S}, \mathcal{Z}), \quad (6)$$

where $\mathcal{T} = (\Lambda_\star, \Lambda_{\text{comp}})$, $\mathcal{S} = (\nu_{s,\star}, \nu_{s,\text{comp}})$, and $\mathcal{Z} = (M_\star, M_{\text{comp}}, R_\star, R_{\text{comp}})$. Here we will not investigate further the dephasing caused by spin coupling effects (spin-orbit, spin-spin, self-spin, etc.), while we note that \mathcal{S} are not dummy as the spins affect the dynamical tides.

A. Analytic Tidal Dephasing

Equilibrium tides are usually addressed by extending the effective gravitational potential in EOB to include an enhancement due to higher-order PN contributions [52, 54], while dynamical tides can be investigated either by introducing associated kinetic terms to the Hamiltonian [14, 59] or by generalising the Love number k_2 to a running parameter (effective tidal responses) [13, 14, 60]. We adopt the PN evolution of binaries together with a kinetic term for dynamical tides to investigate the accumulated tidally-induced dephasing during the pre-merger stage ($f_{\text{gw}} \lesssim 10^3$ Hz). This approach is numerically cheaper while agrees very well with the more sophisticated EOB method (cf. Fig. 1 in [15]; see also Fig. 2). To demonstrate the faithfulness of our code, we will compare our results with several analytical waveforms in this section.

To the leading order of the tidal deformability, the 1

PN order phase shift due to effects of the equilibrium tides in the primary, based on the TaylorF2 model, reads as [8]

$$\Delta\Psi_{\star}^{\text{eq}} = -\frac{3\Lambda_{\star}}{128}(\pi\mathcal{M}f_{\text{gw}})^{-5/3}x^5[a_0 + a_1x] \approx \Psi(f_{\text{gw}}; \mathcal{T}, \mathcal{S}, \mathcal{Z}) - \Psi(f_{\text{gw}}; \mathcal{O}, \mathcal{S}, \mathcal{Z}), \quad (7)$$

where $x = [\pi(M_{\star} + M_{\text{comp}})f_{\text{gw}}]^{2/3}$, $\mathcal{O} = (0, 0)$ denotes a null pair, \mathcal{M} is the chirp mass,

$$\mathcal{M} = \frac{(M_{\star}M_{\text{comp}})^{3/5}}{(M_{\star} + M_{\text{comp}})^{1/5}} = M_{\star}\frac{q^{3/5}}{(1+q)^{1/5}}, \quad (8)$$

and η is the symmetric mass ratio,

$$\eta = \frac{M_{\star}M_{\text{comp}}}{(M_{\star} + M_{\text{comp}})^2}. \quad (9)$$

The coefficient

$$a_0 = 12[1 + 7\eta - 31\eta^2 - \sqrt{1 - 4\eta}(1 + 9\eta - 11\eta^2)], \quad (10a)$$

is the Newtonian contribution, and

$$a_1 = \frac{585}{28} \left[1 + \frac{3775}{234}\eta - \frac{389}{6}\eta^2 + \frac{1376}{117}\eta^3 - \sqrt{1 - 4\eta} \left(1 + \frac{4243}{234}\eta - \frac{6217}{234}\eta^2 - \frac{10}{9}\eta^3 \right) \right], \quad (10b)$$

is the 1 PN one. Although Eq. (7) encodes solely the tide in the primary, the effects from the companion can be linearly added to the gross influence, which can be simplified as [61, 62]

$$\Delta\Psi_{\star}^{\text{eq}} + \Delta\Psi_{\text{comp}}^{\text{eq}} = -\frac{3\tilde{\Lambda}}{128}(\pi\mathcal{M}f_{\text{gw}})^{-5/3}x^5 \times \left[\frac{39}{2} + \left(\frac{3115}{64} - \frac{6595}{364}\sqrt{1 - 4\eta}\frac{\delta\tilde{\Lambda}}{\tilde{\Lambda}} \right)x \right], \quad (11)$$

where

$$\tilde{\Lambda} = \frac{16}{13(M_{\star} + M_{\text{comp}})^5} \left[(M_{\star} + 12M_{\text{comp}})M_{\star}^4\Lambda_{\star} + (M_{\text{comp}} + 12M_{\star})M_{\text{comp}}^4\Lambda_{\text{comp}} \right] \quad (12)$$

is the mutual tidal deformability, and

$$\delta\tilde{\Lambda} = \frac{1}{2} \left[\sqrt{1 - 4\eta} \left(1 - \frac{13272}{1319}\eta + \frac{8944}{1319}\eta^2 \right) (\Lambda_{\star} + \Lambda_{\text{comp}}) + \left(1 - \frac{15910}{1319}\eta + \frac{32850}{1319}\eta^2 + \frac{3380}{1319}\eta^3 \right) (\Lambda_{\star} - \Lambda_{\text{comp}}) \right]. \quad (13)$$

We note that $\delta\tilde{\Lambda}$ is typically much smaller than $\tilde{\Lambda}$, and will vanish for symmetric binaries.

The above 1 PN form can be extrapolated to 2.5 PN with the aid of EOB treatment as shown in [6]; for symmetric binaries, the equilibrium tidal effect of the primary leads to the dephasing

$$\Delta\Psi_{\star}^{\text{eq}} = -\frac{117\Lambda_{\star}}{128}x^{5/2} \left[1 + \frac{3115}{1248}x - \pi x^{3/2} + \frac{28024205}{3302208}x^2 - \frac{4283}{1092}\pi x^{5/2} \right], \quad (14)$$

and can be doubled to include the influence of the companion.

The 2.5 PN correction to the phase acceleration (4) due to tidal contribution, on the other hand, reads as

$$\tilde{Q}_{\omega}^T = -\frac{65}{32}x^{5/3} \left[1 + \frac{4361}{624}x^{2/3} - 4\pi x + \frac{5593193}{122304}x^{4/3} - \frac{4283}{156}\pi x^{5/3} \right], \quad (15)$$

and is given along side the formula for GW phase in [6].

This 2.5 PN TaylorF2 model was later phenomenologically calibrated by numerical relativity simulations in [48] to capture dynamical tidal effects by replacing $\tilde{\Lambda}$ in Eq. (14) with $\tilde{\Lambda}(1 + 12.55\tilde{\Lambda}^{2/3}x^{4.240})$. The authors further show that one can directly generalise the above phase expression, which is for symmetric binaries, to asymmetric systems by substituting the denominator of the pre-factor with 256η , i.e.,

$$\Delta\Psi_{\star}^{\text{eq}} + \Delta\Psi_{\text{comp}}^{\text{eq}} = -\frac{117}{256\eta}x^{5/2}\tilde{\Lambda}(1 + 12.55\tilde{\Lambda}^{2/3}x^{4.240}) \times \left[1 + \frac{3115}{1248}x - \pi x^{3/2} + \frac{28024205}{3302208}x^2 - \frac{4283}{1092}\pi x^{5/2} \right]. \quad (16)$$

Although there is a mutation of 2.5 PN tidal phase approximant derived by Henry et al. [63], which is slightly different from the one in [47] (they match up to 1 PN tidal phasing, i.e., 6 PN effects in general), we will use the above NR-reshaped form for statistical estimation in Sec. III C. In addition to TaylorF2, the NR-calibrated form for TaylorT2 has also been derived in [16], which gives rise to the dephasing

$$\Delta\Psi_{\star}^{\text{eq}} + \Delta\Psi_{\text{comp}}^{\text{eq}} = -\frac{117\tilde{\Lambda}}{64}x^{5/2} \times \frac{1 - 17.428x + 31.867x^{3/2} - 26.414x^2 + 62.362x^{5/2}}{1 + (-17.428 - 3115/1248)x + 36.089x^{3/2}}. \quad (17)$$

Although several models for equilibrium tides have been developed, dynamical tidal dephasing due to the quadrupolar f -mode in the primary is just provided in

[15] recently, given by

$$\Delta\Psi_{\star}^{\text{dyn}} = -\frac{10\sqrt{3}\pi - 27 - 30\log 2}{96\eta}(\pi M_{\star} f_{\text{gw}})^{11/3} \times \frac{\Lambda_{\star} M_{\star}^4 \omega_f^{-2}}{(M_{\star} + M_{\text{comp}})^6} \left(155 - 147 \frac{M_{\star}}{M_{\star} + M_{\text{comp}}}\right), \quad (18)$$

where ω_f is the frequency of the f -mode. This analytical phase shift agrees with the tidal EOB model for $f_{\text{gw}} \lesssim 10^3$ Hz [15].

III. TIDAL DEPHASING: NUMERICAL RESULTS

The Hamiltonian describing the binary evolution is [12, 36, 59]

$$H(t) = (H_{\text{orb}} + H_{\text{reac}} + H_{\text{osc}} + H_{\text{tid}})(t), \quad (19)$$

where H_{tid} and H_{osc} are the Hamiltonians describing the equilibrium and dynamical tidal effects, respectively. We consider the conservative motion, H_{orb} , up to 3 PN level, and include the gravitational back-reaction, H_{reac} , at 2.5 PN order [36]. The explicit forms for the point-particle part of $H(t)$, viz. H_{orb} and H_{reac} , are rather long and are not the subject of the present article, which are thus omitted here but we refer the interested reader to [64, 65]. Nonetheless, we will give the form of the tidal parts $H_{\text{osc}} + H_{\text{tid}}$ in due course, for which the coupling strength of modes to the external tidal field is a crucial parameter (Sec. III A).

The determination of Λ via the phase shift due to equilibrium tides can set constraints on the EOS as demonstrated by the analysis of GW 170817 [10]. However, we need to take also dynamical tides into account since more accurate observations will be available in the next years. This entails a good handle on the QNM effects on the waveforms especially in the high frequency window, where the influence of tidal effects in the GW signal is encoded (cf. Fig. 2 of [66]). Ignoring the dynamical tide contribution in the phase shift will therefore deteriorate the accuracy in constraining the EOS. Furthermore, for binaries involving rapidly-rotating NSs the effect will be more pronounced since the f -mode frequency will be lowered, leading into larger tidal dephasing. In this article, we consider the GW phase accumulated when f_{gw} ranges between $f_{\text{min}} = 20$ Hz and $f_{\text{max}} = 1000$ Hz, given by

$$\Psi_{\text{tot}} = \int_{f_{\text{min}}}^{f_{\text{max}}} df_{\text{gw}} \left(\frac{\partial \Psi}{\partial f_{\text{gw}}} \right)_{\Lambda_{\star}, \Lambda_{\text{comp}}, \nu_{s,\star}, \nu_{s,\text{comp}}} = \Psi_{\text{pp}} + \Delta\Psi^T. \quad (20)$$

Here Ψ_{pp} is the part of point-particle contribution, and $\Delta\Psi^T$ is the tidal dephasing due to both equilibrium and dynamical tides.

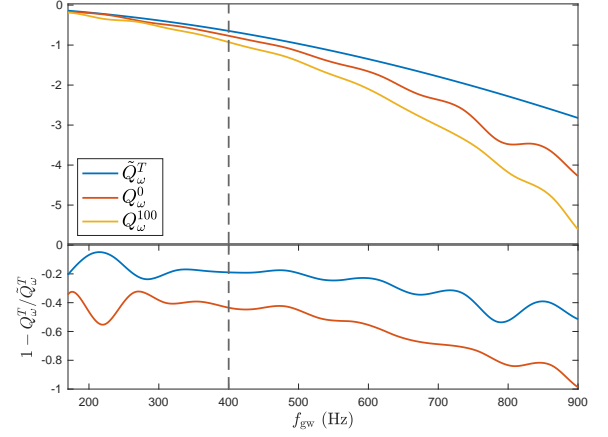


FIG. 1. Ratio between the numerically estimated phase acceleration $Q_{\omega}^T = \{Q_{\omega}^0, Q_{\omega}^{100}\}$ [Eq. (4)] and the analytic 2.5 PN form \tilde{Q}_{ω}^T [Eq. (15)].

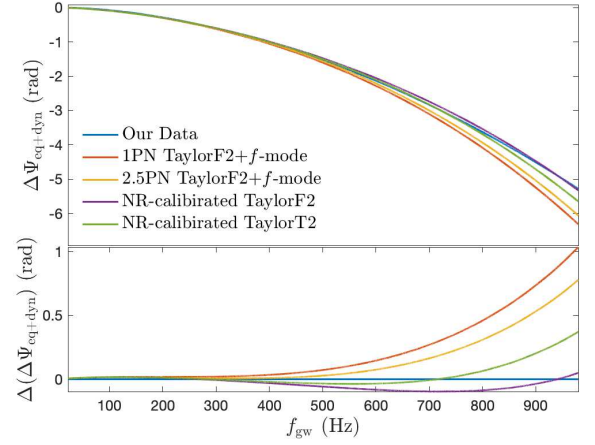


FIG. 2. Tidal dephasing, including equilibrium and dynamical tides, from our code (blue) and several analytic models (see the main text) as functions of f_{gw} . For this plot, we consider a symmetric binary with $M_{\text{comp}} = 1.3M_{\odot} = M_{\text{comp}}$ and MPA1 EOS [67]. The results shown here account only for the tides in the primary, thus the total effect is twice as big.

In Fig. 1, we compare our result of phase acceleration Q_{ω}^0 , for a particular symmetric binary with a non-spinning primary, with \tilde{Q}_{ω}^T given by Eq. (15). We see that our result, which includes the f -mode effect, has a deviation $\leq 20\%$ from the analytic result for $f_{\text{gw}} < 500$ Hz, while larger deviation is observed for high frequencies. The growing deviation can be attributed to f -mode excitation, which is absent in the analytic expression (15). To demonstrate that the deviation originates from the presence of f -mode, we add in the plot the phase acceleration Q_{ω}^{100} , for the same binary but with the primary spinning at 100 Hz. The enhanced f -mode effect in the latter spinning case manifests as the larger deviation from Eq. (15).

In addition, the inclusion of f -mode effect gives rise to a more negative phase acceleration, suggesting a faster merging (the so-called “tidally induced plunge” [12]).

On the other hand, in Fig. 2, the GW phase of our simulation (blue curve) is compared to the following approaches: (i) 1 PN TaylorF2 + f -mode [Eq. (11) and Eq. (18)], (ii) 2.5 PN TaylorF2 + f -mode [Eq. (14) and Eq. (18)], (iii) NR-calibrated TaylorF2 [Eq. (16)], and (iv) NR-calibrated TaylorT2 [Eq. (17)]. Denoting the difference between our tidal phase shift to a certain model as $\Delta(\Delta_{\text{eq+dyn}}) = \Delta_{\text{eq+dyn}}^{\text{ours}} - \Delta_{\text{eq+dyn}}^{\text{model}}$, we see that the deviation from the aforementioned models is less than 1 rad overall, and most of the deviation piles up after $f_{\text{gw}} \gtrsim 400$ Hz. Our numerical scheme produces smaller dephasing compared to the two non-NR-corrected models, meaning the tidal effect in our scheme is a bit weaker. However, the shifts are greater than those of NR-calibrated models when f_{gw} is less than a certain value. This “sign-changing” behaviour is often seen when it comes to comparing different waveform models (e.g., [15, 49, 68]). Among the considered models, the model using TaylorF2 with NR waveforms fits to our result the best with difference only between ± 0.1 rads.

As the QNM spectrum depends on EOS and spin, we will address how these affect the tidally-induced phase shift, notably the dependence on EOS (Sec. III A) and the tidal effects of spinning stars (Sec. III B). In general the spin itself will lead to certain dephasing due to, e.g., spin-orbit, spin-spin, and self-spin couplings. The total dephasing thus consists of the tidal and spin-included contributions. Identifying of tidal part accurately is crucial in acquiring source parameters; some discussion on this issue will be provided at the end. Before we investigate the aforementioned aspects, we first attain confidence on the results of our code by comparing with the analytic forms obtained via PN expansions, the EOB scheme, and the phenomenological models fitting to NR simulations.

A. An EOS-independent Tidal Hamiltonian

In general, stellar oscillations in GR will cause perturbations in metric fields, thus damping in a certain timescale set by the imaginary part of mode frequencies. However, we are studying the very last moment of coalescence, where the few minutes is not enough for modes to decay. Therefore, we ignore the small contributions from the mode-induced metric perturbation and from the imaginary part of the mode in the tidal parts of Hamiltonian, which then has the form (cf. Eqs. (16) and (25)

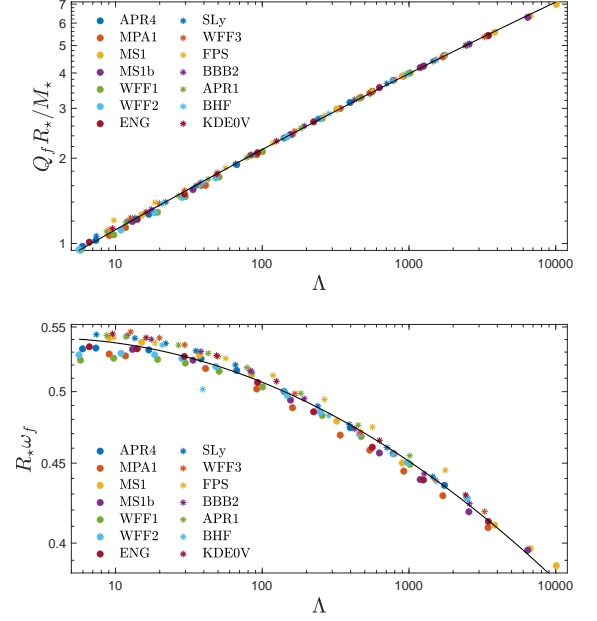


FIG. 3. Universal relations connecting $Q_f R_*/M_*$ [Eq. (25); top panel] and $R_*^2 \omega_f^2$ [Eq. (24); bottom panel] to the tidal deformability of the primary Λ_* .

in [36])

$$H_{\text{tid}} = -\frac{2M_* M_{\text{comp}}}{a R_*} \sum_{\alpha} W_{lm} \left(\frac{R_*}{a} \right)^l \Re [\bar{q}_{\alpha} Q_{\alpha} e^{-im\phi_c}], \quad (21)$$

$$H_{\text{osc}} = \frac{1}{2} \sum_{\alpha} \left(\frac{p_{\alpha} \bar{p}_{\alpha}}{M_* R_*^2} + M_* R_*^2 \sigma_{\alpha}^2 q_{\alpha} \bar{q}_{\alpha} \right) + \text{H.c.}, \quad (22)$$

where we focus on the tidal activity in the primary. Here α labels different QNMs, ϕ_c is the phase coordinate of the companion, q_{α} are the mode amplitudes, and p_{α} are the canonical momenta associated to q_{α} . The (inertial-frame) eigenfrequency of the excited mode is $\sigma_{\alpha} = \omega_{\alpha} + i/\tau_{\alpha}$, where ω_{α} is the frequency, and τ_{α} the damping timescale. The overhead bar denotes complex conjugation. As stated above, we will limit our study to the $l = 2 = m$ f -mode hence we will drop the subscript α hereafter, and denote its coupling strength as Q_f , which should not be confused with the phase acceleration Q_{ω} defined in Eq. (4).

We introduce the primary-based, dimensionless quantities

$$\mathcal{A}(\Lambda_*) = Q_f R_*/M_*, \quad (23a)$$

$$\mathcal{B}(\Lambda_*) = R_* \omega_f, \quad (23b)$$

which, if the primary is non-spinning (i.e., ω_f is the mode frequency), can be expressed as functions of Λ . In particular, we find the universal relations for these two

quantities, given by

$$\log \mathcal{A} = -0.250 + 0.306 \log \Lambda_\star - 0.008 (\log \Lambda_\star)^2, \quad (24)$$

and

$$\log \mathcal{B} = -0.270 + 0.013 \log \Lambda_\star - 0.013 (\log \Lambda_\star)^2. \quad (25)$$

The relations are plotted in Fig. 3, where the considered set of EOS is labeled in the legend. This set of EOS is the same as those adopted in [69], and we note that the latter formula (25) has been introduced there. The former universal relation connects the tidal overlap of f -mode to the tidal deformability, which is newly pointed out here, while that for r -mode has been developed in [70] (see the right panel of Fig. 7 therein).

Substituting the previous quantities into the tidal Hamiltonian, we get

$$H^T = H_{\text{tid}} + H_{\text{osc}} = -\frac{2M_\star^2 M_{\text{comp}}}{a^3} \mathcal{A} q \cos(m\varphi_c) + \frac{p\bar{p}}{M_\star R_\star^2} + M_\star q \bar{q} \mathcal{B}^2. \quad (26)$$

which is a functional depending on the individual masses M_\star and M_{comp} , the tidal deformability of the primary Λ_\star , and $M_\star R_\star^2$. The latter quantity is related to moment of inertia [71] [see Eq. (12) therein]. The dependencies are all detectable in GW analysis either directly or indirectly; the measurement of the chirp mass \mathcal{M} and the symmetric mass ratio η determine the individual masses, while the measurement of $\tilde{\Lambda}$ returns R_\star in a manner independent of the M_{comp} if the chirp mass is known [72, 73]. In addition, the mass ratio together with $\tilde{\Lambda}$ estimate the individual tidal deformabilities since Λ_\star and Λ_{comp} relate to each other by (see Eq. 8 of [74])

$$\Lambda_\star \simeq q^6 \Lambda_{\text{comp}}. \quad (27)$$

The tidal Hamiltonian can therefore be *EOS-independently reconstructed* from \mathcal{M} , η , and $\tilde{\Lambda}$. The “hierarchy” of the three arguments in GW phasing goes from the chirp mass to the tidal deformability.

In Fig. 4, we plot the accumulated GW phase from $f_{\text{gw}} = 20$ Hz to $f_{\text{gw}} = 1000$ Hz for binaries with fixed chirp mass $\mathcal{M} = 1.186 M_\odot$ as functions of M_\star for some EOS. We note that the chosen EOS span a wide range of stiffness going from the stiffest MPA1 down to the softest KDE0V. The binaries considered in Fig. 4 undergo ~ 2260 orbits in the last ~ 150 s of the coalescence, during which f_{gw} climbs from 20 Hz to 10^3 Hz. This corresponds to ~ 4560 cycles of *time-domain* gravitational waveform, while the *frequency-domain* gravitational waveform (1) is found to oscillate ~ 4775 cycles, i.e., $\Psi_{\text{tot}} \lesssim 3 \times 10^4$ rads. The phase varies $\lesssim 1\%$ for different η , while the variance of the finite size effects encoded in $\tilde{\Lambda}$ is even smaller. Following the EOS-independent nature of the Hamiltonian, the accumulated phase is thus, to a large degree, uncorrelated to the

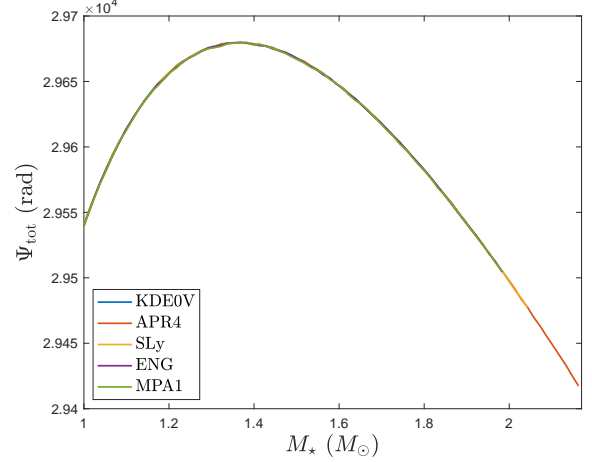


FIG. 4. Ψ_{tot} [Eq. (20)] for binaries with a fixed chirp mass $\mathcal{M} = 1.186 M_\odot$ as functions of M_\star for the chosen EOS. Each curve terminates at the maximal mass of the associated EOS.

EOS. To our knowledge, the universality of the GW phase shift when fixing the chirp mass has not yet been recognised in the literature. In addition, the phase peaks at $M_\star = M_{\text{comp}} \simeq 1.37 M_\odot$, indicating that symmetric binaries will undergo more cycles before merger regardless the stellar constitution.

Although this Hamiltonian is EOS-independent, it is not indicating that we cannot place any constraints on EOS from the GW phasing detection. On the contrary, from the analysis of GW phase, we may determine the properties of the binary members to place certain constraints on EOS, e.g., the predicted $\tilde{\Lambda}$ of GW170817 favours soft candidates.

B. Spin modification in Tidal Dephasing

In spinning neutron stars the oscillation frequency splits into co- and counter-rotational components. In the inertial frame, the f -mode frequency, ω_f , of the primary shifts according to (cf. Eq. (70) in [36])

$$\delta\omega_f^R = 2\pi m(1 - C_f)\nu_{s,\star}, \quad (28)$$

where C_f depends on the eigenfunction of f -mode via the integration of Eq. (71) in [36]. For a fast-rotating primary, the frequency shift formulae involving extra terms quadratic in $\nu_{s,\star}$ has been proposed in [75–77]. This quadratic term is however negligible up to high spin $\nu_{s,\star} \gtrsim 800$ Hz, and the linear modification shown in Eq. (28) is adequate for our purpose. The counter-rotating shift in the frequency of the $l = 2 = -m$ f -mode is always negative since $C_f \approx 0.3$. A smaller oscillation frequency indicates an earlier resonant coupling between the mode and the orbital frequency, thus the accumulation of tidal effects in the waveform will be more significant.

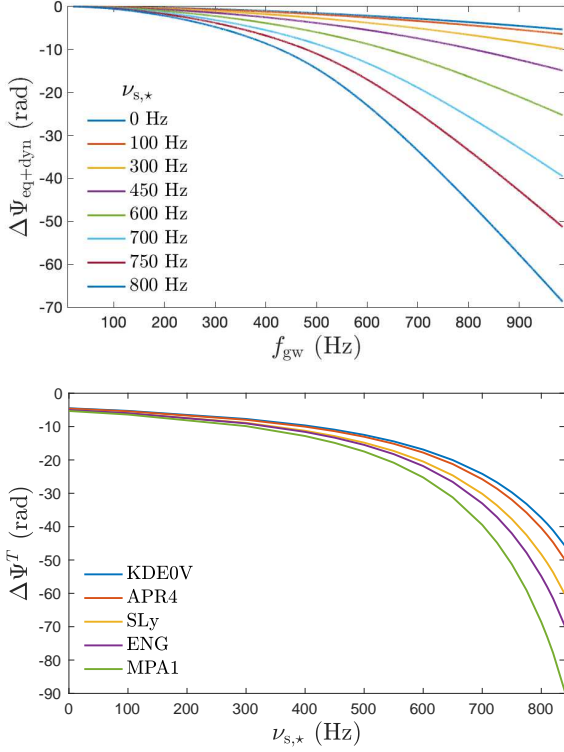


FIG. 5. *Top panel:* Evolution of GW phase for various spin rates of the primary, $\nu_{s,*}$, as functions of f_{gw} for a particular binary (we assumed the MPA1 EOS). *Bottom panel:* Accumulated phase shift $\Delta\Psi^T$ due to tidal effects in both NSs as a function of $\nu_{s,*}$, here we used the same EOS as in Fig. 4. For both panels, we consider the tidal effect of the primary in symmetric binaries.

For particular symmetric binaries with two NSs spinning at the same rate and having the same mass, we plot in the top panel of Fig. 5 the tidal dephasing induced by the primary for various spins, as functions of f_{gw} . We see that the phase shift increases monotonically with $\nu_{s,*}$, while a noticeable, rapid growth is observed in the high GW frequency regime. For instance, the dephasing piles up to about 20 rads for the case with $\nu_{s,*} = 800$ Hz during $f_{\text{gw}} < 500$ Hz, while the accumulated dephasing is $\lesssim 150$ rad from $f_{\text{gw}} = 500$ to 10^3 Hz. In the bottom panel of Fig. 5, we show the tidal dephasing $\Delta\Psi^T$ defined in Eq. (20) as function of $\nu_{s,*}$ for the five EOS used in Fig. 4. We observe that the waveform dephasing depends on the EOS, and is smaller for softer EOS due to the smaller radius of the star. Again, we witness a rapid increase of $|\Delta\Psi^T|$ for higher spin due to a different reason. For cases with fixed spin, the dephasing grows faster for a cutoff $f_{\text{max}} > 500$ Hz since the information of dynamical tides lies in the high frequency part of waveforms; on the other hand, for cases assuming a fixed f_{max} , the dephasing enlarges due to early excitation of f -mode. In particular, a tidal correction of for $f_{\text{max}} = 10^3$ Hz and $\nu_{s,*} = 850$ Hz, the dephasing of $\Delta\Psi^T \lesssim 100$ rad [right end of the green curve in the bottom panel of Fig. 5] is

mainly caused by f -mode excitation since the contribution of the equilibrium tide is only $\lesssim 10$ rad.

In addition, we find that there exists a universal relation between $\Delta\Psi^T$ and the dimensionless spin $\nu_{s,*}M_{\star}^2/R_{\star}$, given by

$$\begin{aligned} \Delta\Psi^T = & -4.850 - 2.539 \times 10^{-2}\tilde{\nu} + 2.449 \times 10^{-4}\tilde{\nu}^2 \\ & - 1.429 \times 10^{-6}\tilde{\nu}^3 + 3.026 \times 10^{-9}\tilde{\nu}^4 \\ & - 2.482 \times 10^{-12}\tilde{\nu}^5 \text{ rad} \end{aligned} \quad (29)$$

for a normalised spin

$$\tilde{\nu} = \nu_{s,*} \left(\frac{M_{\star}}{1.2M_{\odot}} \right)^2 \left(\frac{R_{\star}}{12 \text{ km}} \right). \quad (30)$$

The relation (29) is plotted in Fig. 6.

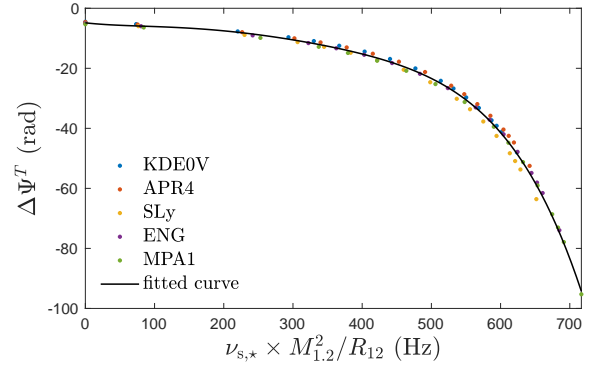


FIG. 6. Tidal dephasing as a universal function of the dimensionless, normalised spin defined in Eq. (30).

Although the EOS-independent Hamiltonian (26) is allowed by a non-spinning primary, its universality survives for spins $\nu_{s,*} \lesssim 100$ Hz. For example, we see that the phase shift $\Delta\Psi^T$ is EOS-independent for $\nu_{s,*} \lesssim 100$ Hz (bottom panel of Fig. 5). In reality, mode frequency will be modified differently depending on the EOS. Although this difference is minor for small spins, the dependence of the phase shift on the EOS is becoming observable as the stellar spin increases.

The Hamiltonian is EOS-independent for most of the coalescing NS binaries since its members are typically old and tend to rotate slowly. Nevertheless, there may still be a number of NSs in binaries with moderate and higher spin rates. A potential case is the secondary of GW190814 [78], we will discuss the specific case in we will Sec. IV.

Apart from the rotation-induced modifications to the f -mode frequency ω_f , rotation will induce a correction δQ_f to the tidal overlap integral Q_f . This term, however, is of quadratic order to $\nu_{s,*}$ [79, 80], and is typically $\delta Q_f \lesssim 10^{-3}Q_f$ even for the fastest rotating NS in a binary observed to-date, viz. PSR J0737-3039A, whose dimensionless spin is $\chi \lesssim 0.05$ (~ 44 Hz; [81]). However, the secondary of GW190814 has a finite chance to set a

new record with $\chi \sim 0.47$ (~ 1170 Hz [41]; see also below). In the latter system, a correction of $\delta Q_f \gtrsim 0.2Q_f$ is expected. However, we will not explore this interesting case in the present article, and we will base our estimations on the tidal overlap integral for non-rotating stars.

C. Statistical Error

The phase of the (frequency-domain) GW waveform is particularly crucial in estimating parameters in the matching filter algorithm [3, 37, 82], which we summarise in the following.

Defining a sensitivity-curve-weighted inner product in the waveform-space as

$$(g|h) = 2 \int_0^\infty \frac{g^*(f)h(f) + h(f)^*g(f)}{S_n(f)} df, \quad (31)$$

for two frequency-domain waveforms f and g , the SNR can then be express as

$$\rho^2[h] = (h|h) = 4 \int_0^\infty \frac{|h(f)|^2}{S_n(f)} df = 4\mathcal{A}^2 \int_0^\infty \frac{f^{-7/3}}{S_n(f)} df, \quad (32)$$

where h is the input waveform template, and the latter equality holds if SPA (1) has been adopted. Here $S_n(f)$ is the sensitivity curve set by the detector, and the superscript asterisk denotes complex conjugate.

As any measurement comes along with errors, we have to handle the posterior possibility of getting a somewhat different set of parameters θ , which deviates from the true parameters θ_o , by a minute inaccuracy $\Delta\theta_o$ for a given signal s , i.e., $p(\theta|s)$ must be under controlled. For a large S/N , the approximation for the posterior possibility,

$$p(\theta|s) \propto \exp \left[-\frac{1}{2} \Gamma_{ab} \Delta\theta^a \Delta\theta^b \right], \quad (33)$$

exhibits a Gaussian distribution around θ_o [3, 4], which is characterised by the Fisher information matrix

$$\Gamma_{ab} = \left(\frac{\partial h}{\partial \theta^a} \middle| \frac{\partial h}{\partial \theta^b} \right). \quad (34)$$

The measurement error of θ^a is then defined as

$$\sigma_a = \sqrt{(\Gamma^{-1})^{aa}}, \quad (35)$$

where Γ^{-1} is the inverse of the Fisher matrix.

Neglecting explicitly spin-related terms, which is appropriate when the spin is well-constrained (see discussion) or rather small² [6], we have the symbolic expression

$$h = h(f_{\text{gw}}; \mathcal{A}, f_0 t_o, \phi_o, \mathcal{M}, \eta, \tilde{\Lambda}, \omega_f) \quad (36)$$

focusing on the explicit dependencies. Here f_0 is the frequency at the minimum of the sensitivity curve, and we recall that t_o and ϕ_o are the reference time and phase often set as the values of as of merger [defined in Eq. (2)]. Although the Fisher matrix is 7 dimensional, we can suppress one of its dimensions by factoring out the elements related to \mathcal{A} since the amplitude is uncorrelated with the other quantities involved in the inner product Eq. (31) in SPA.

For the measurement of \mathcal{M} and η , it has been demonstrated in [6] that 2 PN order approximants for point-mass waveform suffice the purpose of estimating errors in tidal parameters. For later convenience, we provide the derivatives (cf. Eq. (3.10) of [4])

$$\frac{\partial \ln h_{\text{pp}}}{\partial (f_0 t)} = 2\pi i (f_{\text{gw}}/f_0), \quad (37a)$$

$$\frac{\partial \ln h_{\text{pp}}}{\partial \phi_o} = -i, \quad (37b)$$

$$\frac{\partial \ln h_{\text{pp}}}{\partial \ln \mathcal{M}} = -\frac{5i}{128} (\pi \mathcal{M} f_{\text{gw}})^{-5/3} \left[1 + \left(\frac{743}{252} + \frac{11}{3} \eta \right) x - \frac{32\pi}{5} x^{3/2} + \left(\frac{3058673}{508032} + \frac{5429}{504} \eta + \frac{617}{72} \eta^2 \right) x^2 \right], \quad (37c)$$

and

$$\frac{\partial \ln h_{\text{pp}}}{\partial \ln \eta} = -\frac{i}{96} (\pi \mathcal{M} f_{\text{gw}})^{-5/3} \left[\left(\frac{743}{168} - \frac{33}{4} \eta \right) x - \frac{108}{5} \pi x^{3/2} + \left(\frac{3058673}{56448} - \frac{5429}{224} \eta - \frac{5553}{48} \eta^2 \right) x^2 \right] \quad (37d)$$

² As of the time this article is prepared, the known, fastest spinning NS in binaries is PSR J0737-3039A, whose dimensionless spin,

though depending on the EOS, is estimated to be $\lesssim 0.03$ [6].

TABLE I. Statistical estimation of the measurement error for the accumulated tidal dephasing $\Delta\Psi^T$ [Eq. (20)] (3rd column), the GW phase $\Delta\phi_o$ (4th column), the chirp mass $\Delta\mathcal{M}/\mathcal{M}$ (5th column), the symmetric mass ratio $\Delta\eta/\eta$ (6th column), the mutual tidal deformability $\Delta\tilde{\Lambda}/\tilde{\Lambda}$ (7th column), and the frequency of the f -mode in the primary $\Delta\omega_f/\omega_f$ (8th column) assuming the cutoff as $f_{\max} = 10^3$ Hz. We additionally considered the uncertainty of $\tilde{\Lambda}$ for $f_{\max} = 450$ Hz in the final column so as to be compared to the results in [6], which are shown in the final column of their Tab. 2 though there the authors adopted $\rho = 1$ and did not present by percentage. We assumed symmetric binaries with $\tilde{\Lambda} = 920$ while the EOS used are listed in the 1st column. We used four representative spin rates (given in Hz): 0 (non-spinning), 45 (fastest known NS in binaries), 500 (moderate fast), and 800 (rather fast) of the primary. In general, the errors scale as $1/\rho$, while the results derived assuming an SNR value of $\rho = 25$. The table are prepared by considering only the tidal effects of the primary.

EOS	$\nu_{s,*}$ (Hz)	$\Delta\Psi^T$ (rad)	$\Delta\phi_o$ (rad)	$\Delta\mathcal{M}/\mathcal{M}$	$\Delta\eta/\eta$	$\Delta\tilde{\Lambda}/\tilde{\Lambda}$	$\Delta\omega_f/\omega_f$	$[\Delta\tilde{\Lambda}/\tilde{\Lambda}]_{450}$
KDE0V	0	-4.4982	1.5231	0.0037%	1.1383%	5.0868%	664.5%	83.67%
	45	-4.8299	1.5150	0.0037%	1.1335%	4.4050%	568.3%	73.23%
	500	-12.4849	1.6379	0.0038%	1.2128%	0.6339%	74.08%	5.940%
	800	-37.3150	1.4969	0.0037%	1.1274%	0.2266%	14.92%	2.080%
APR4	0	-4.5928	1.5220	0.0038%	1.1496%	4.8817%	634.9%	79.62%
	45	-4.9372	1.5138	0.0038%	1.1447%	4.2180%	541.5%	69.74%
	500	-13.0437	1.4196	0.0037%	1.0886%	0.7189%	70.23%	11.99%
	800	-40.4013	1.5165	0.0038%	1.1514%	0.2151%	13.79%	1.777%
SLy	0	-5.0406	1.5218	0.0039%	1.1630%	4.3130%	557.2%	69.71%
	45	-5.4287	1.5137	0.0039%	1.1581%	3.7168%	473.6%	60.76%
	500	-14.8164	1.4367	0.0038%	1.1124%	0.6322%	60.40%	9.857%
	800	-48.2919	1.5813	0.0040%	1.2057%	0.1956%	12.18%	1.300%
ENG	0	-5.0167	1.5184	0.0042%	1.1828%	4.1548%	531.8%	66.64%
	45	-5.4175	1.5110	0.0042%	1.1782%	3.5738%	450.8%	57.58%
	500	-15.4857	1.4449	0.0041%	1.1388%	0.5933%	54.78%	8.660%
	800	-54.8652	1.6344	0.0044%	1.2623%	0.1858%	10.93%	0.9655%
MPA1	0	-5.3222	1.5179	0.0045%	1.2083%	3.7394%	473.2%	58.69%
	45	-5.7651	1.5102	0.0045%	1.2034%	3.2010%	398.6%	49.91%
	500	-17.4710	1.2997	0.0042%	1.0679%	0.6222%	17.48%	14.19%
	800	-68.6082	1.7409	0.0049%	1.3587%	0.1700%	9.410%	0.6029 %

for the point-mass approximants. We will approximate the variance of the strain (36) with infinitesimal changes of non-tidal parameters by the point-mass formulas (37), i.e.,

$$\frac{\partial h}{\partial X} \simeq \frac{\partial h_{\text{pp}}}{\partial X} \quad (38)$$

for $X = \{f_0 t, \phi_o, \ln \mathcal{M}, \ln \eta\}$. On the other hand, we numerically evaluate $\frac{\partial h}{\partial \tilde{\Lambda}}$ by first constructing two waveforms with slightly different tidal deformabilities $\tilde{\Lambda} \pm \epsilon$, while fixing other parameters, then dividing the difference of the two waveforms by the difference in $\tilde{\Lambda}$, viz.

$$\frac{\partial h}{\partial \tilde{\Lambda}} = \frac{h(\tilde{\Lambda} + \epsilon) - h(\tilde{\Lambda} - \epsilon)}{2\epsilon}. \quad (39)$$

The scheme admits that the variation of $h(\Lambda)$ does not feel the variance of the others (even though via the inversion of the Fisher matrix there is some mixing). The

same procedure is performed for the parameter ω_f to obtain $\partial h / \partial \omega_f$. Measurement errors, (35), can then be calculated by inverting the Fisher matrix (34).

Adopting the sensitivity curve of aLIGO and assuming that the data streams are measured across the frequency band $20 \leq f_{\text{gw}} \leq 10^3$ Hz with a SNR $\rho = 25$, we estimate the errors $\Delta\mathcal{M}/\mathcal{M}$, $\Delta\eta/\eta$, $\Delta\tilde{\Lambda}/\tilde{\Lambda}$ and $\Delta\omega_f/\omega_f$ in Table I. We see that the magnitude of tidal phase shift $\Delta\Psi^T$ increases with stellar spin due to earlier excitation of f -mode, allowing for a more accurate extraction of tidal parameters. In particular, the error in $\tilde{\Lambda}$ and ω_f reduce rapidly for increasing spin, where the error can be $< 1\%$ for the former and $< 15\%$ for the latter if the NS spins at 800 Hz. The improvement in the measurability of both $\tilde{\Lambda}$ and ω_f is due to the earlier excitation of the f -mode whose frequency was shifted by the rotation. An earlier mode excitation increases significantly the transfer of orbital energy to stellar oscillations affecting significantly the dephasing. As a result, f -mode frequency will be estimated with significantly smaller error. Actually,

even though the dephasing due to the equilibrium tide is not directly affected, the increasing influence of the dynamical tides encodes certain information of the equilibrium tides since the latter is the adiabatic limit of the former – notice that Λ factors out in $\Delta\Psi_{\star}^{\text{dyn}}$ in Eq. (18). Therefore, by including the dynamical tides in the Fisher analysis for Λ we effectively place extra emphasis on the high-frequency part of waveform.

For the considered data stream, the tidal dephasing $\Delta\Psi^T$ is larger than the uncertainty of phase $\Delta\phi_o$ even for a non-spinning star. However, the tidal dephasing may be hidden in the uncertainty in phase $\Delta\phi_o$ for a lower cutoff. In general, tidal dephasing is a function of $\nu_{s,\star}$ and f_{max} [i.e., $\Delta\Psi_T = \Delta\Psi_T(\nu_{s,\star}, f_{\text{max}})$], while the uncertainty in phase is a function of SNR and f_{max} [i.e., $\Delta\phi_o = \Delta\phi_o(\rho, f_{\text{max}})$]. For a particular binary with the spin of the primary being $\nu_{s,\star} = 45$ Hz and the SNR of the associated waveform being $\rho = 25$, we integrate Eq. (20) and Eq. (31) from $f_{\text{gw}} = 20$ Hz to a varying cutoff f_{max} . We plot $\Delta\phi_o$ and $\Delta\Psi^T$ as functions of f_{max} in the top panel of Fig. 7. In this example, the tidal dephasing becomes noticeable if the cutoff is $\gtrsim 600$ Hz. In general setting, there is a minimal SNR ρ_{thr} for a specific spin ν_o and cutoff $f_{\text{max},o}$, defined by the equality

$$\Delta\Psi^T(\nu_o, f_{\text{max},o}) = \Delta\phi_o(\rho_{\text{thr}}, f_{\text{max},o}). \quad (40)$$

To grasp how the increasing spin improves the detectability of tidal effects, we find ρ_{thr} as function of the NS spin assuming some cutoff frequencies for a particular binary in the bottom panel of Fig. 7. Improvement of measurability is observed when f_{max} is extended.

IV. CASE STUDY: GW190814

The event GW190814, reported by the LIGO-Virgo-Kagra collaboration at a SNR of $\rho = 25$ [83], consists of one black hole, weighting $22.2 - 24.3M_{\odot}$, and a compact object with $2.50 - 2.67M_{\odot}$. The mass of the latter intriguingly falls in the so-called “lower mass gap” ($2.5 - 5M_{\odot}$), and may be either the lightest black hole or the heaviest NS known to-date. A possibility that the secondary is a mass-gap, fast-rotating NS has been raised in [39–41], with the highest suggested spin being $\nu_{s,\star} \sim 1170$ Hz [41]. Although the spin parameter for this presumably, rapidly-rotating NS has not been well constrained, an estimation of the dimensionless spin χ via the relation (cf. Eq. (3) of [78]),

$$\chi \approx 0.4 \left(\frac{\nu_{s,\star}}{10^3 \text{ Hz}} \right), \quad (41)$$

gives $\chi \approx 0.47$ for the rate $\nu_{s,\star} \sim 1170$ Hz, which is about 65% of maximum spin ($\chi \sim 0.7$) attainable by an isolated NS [84]. This peculiar system may originate from a dynamical process, such as dynamical encounters in a star cluster [85, 86], hierarchical triple system [87],

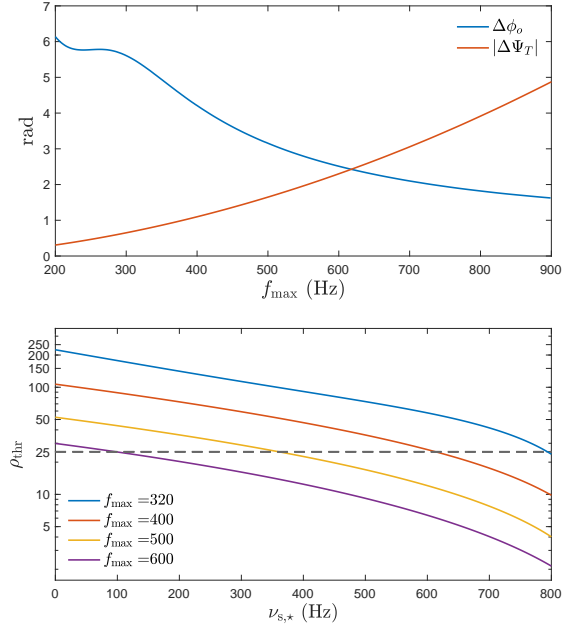


FIG. 7. *Top panel:* Uncertainty in the GW phase $\Delta\phi_o$ (blue) and tidally-induced phase shift $\Delta\Psi^T$ (red) [Eq. (20)] as functions of the cutoff frequency f_{max} . The spin of the primary and the SNR are set as, respectively, $\nu_{s,\star} = 45$ Hz and $\rho = 25$. *Bottom panel:* SNR ρ_{thr} for the uncertainty in phase $\Delta\phi_o$ to equate the tidal dephasing $|\Delta\Psi^T|$ [Eq. (40)] for four cutoff frequencies as functions of $\nu_{s,\star}$. In both panels, the symmetric binary with $\tilde{\Lambda} = 920$ and EOS MPA1 is considered.

and tidal capture [88] of a natal NS kicked off from its born site by a BH.

Compared to the other tidal contributions, dephasing due to spin effects is secondary. Still, it seems that the estimation of spin parameter via its impact on the tidal dephasing may be promising. In this section, we discuss the tidally-induced phase shift for a fast-spinning NS, and estimate how can we probe both the f -mode frequency and the stellar spin rate from the waveform of GW190817 if the secondary turns out to be a fast-rotating NS. We will focus on the tidal dephasing caused by the fast spinning secondary, which is taken as the primary.

A. Estimation of Source Parameters

Adopting the definition of the onset of the merger as [89], i.e., when $\pi(M_{\star} + M_{\text{comp}})f_{\text{gw}} = 0.2$, the total mass of $\sim 27M_{\odot}$ of GW190814 suggests that the merger occurred at $f_{\text{gw}} \lesssim 360$ Hz. In our simulation of the binary having two constituents with the masses and radii of those for GW190814, we find the separation between the two bodies is ~ 95 km when $f_{\text{gw}} = 360$ Hz, which is larger than the sum of the two radii, viz. ~ 75 km. We therefore set the cutoff at $f_{\text{max}} = 360$ Hz and the “competition” between $\Delta\Psi^T$ and $\Delta\phi_o$ is plotted in Fig. 8. We see that the tidal dephasing in the waveform is exceeding the er-

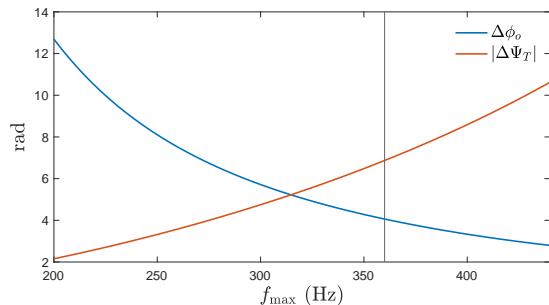


FIG. 8. Same plot as the top panel of Fig. 7, while the spin of the primary is $\nu_{s,*} = 800$ Hz here. The vertical line marks the merger frequency 360 Hz.

ror of phase even with this low cutoff since the spin is rather fast. Ignorance of the tidal effect in this case will therefore deteriorate the extraction of source parameters to an extent worse than ignoring the uncertainty in the reference phase ϕ_o .

Although we show that the inclusion of tidal dephasing is necessary since the primary spins rapidly, the uncertainties for $\tilde{\Lambda}$ and ω_f are however large for this low f_{\max} . We investigate the uncertainties of these two parameters as functions of f_{\max} in a neighbourhood of 360 Hz. In particular, we find the following relations

$$\frac{\Delta\omega_f}{\omega_f} = a_1 \left(\frac{f_{\max}}{360 \text{ Hz}} \right)^{a_2} \%, \quad (42a)$$

and

$$\frac{\Delta\tilde{\Lambda}}{\tilde{\Lambda}} = b_1 \left(\frac{f_{\max}}{360 \text{ Hz}} \right)^{b_2} \%, \quad (42b)$$

for the chosen EOS and $f_{\max} \in [200, 400]$ Hz, where the fitting parameters a_i and b_i are listed in Tab. II. The b_2 parameter is consistent with the trend showed in the Fig. 10 of [48].

Although we have assume the knowledge of the spin in the above analysis, we note that we may estimate the spin by exploiting the universality of the tidal dephasing as a function of the dimensionless spin [Fig. 6; Eq. (29)], together with the mass measurement and the radius inferred by $\tilde{\Lambda}$ in the fashion of [72].

V. DISCUSSION

The phase of gravitational waveform is sensitive to several stellar parameters, which elevates it into an invaluable position in the GW physics era. Among other factors, the tidal contribution to the GW phasing encodes the details of internal motions of NSs, consisting of the equilibrium tide, described by the tidal deformability (Sec. II A), and the dynamical, f -mode oscillation, captured by the mode frequency ω_f and its coupling strength

TABLE II. Parameters relevant to Eq. (42) for the chosen EOS. The inertial-frame, spin-modified f -mode frequency is listed in the second column, and the fitting parameters defined in Eq. (42) are presented from the third to the final column. Here we assume $\nu_{s,*} = 800$ Hz.

EOS	$\omega_f/2\pi$ (Hz)	a_1	a_2	b_1	b_2
KDE0V	817.57	509.55	-2.46	9.05	-2.34
APR4	789.65	436.70	-2.49	7.86	-2.36
SLy	748.47	321.41	-2.53	5.91	-2.38
ENG	697.92	241.25	-2.60	4.59	-2.42
MPA1	637.01	151.46	-2.70	3.04	-2.47

to the external tidal field Q_f [Eq. (21)].

As we mention earlier, both spin and tidal effects will influence the GW phasing though the spin contribution is smaller [90]. Therefore, it is crucial to estimate the phase shift caused by each one of them for the precise estimation of the tidal parameters (e.g., [24]). If we can determine independently the stellar spin through, e.g., the range of dynamical ejecta [91, 92], a shift in the main pulsating mode in hypermassive NS remnant [93, 94], or a system showing double precursors [95], we can construct a point-particle waveform for that spin. Subtracting the point-particle waveform from the data then returns the tidal dephasing. In addition, the tidal effects are encoded in the high frequency part of GW data stream, while the spin affects mainly the low frequency part [28, 66]. We may acquire the individual spins in the early waveform by firstly measuring the mutual, effective spin via spin-orbit contribution in GW phase shift, then solving for the individual ones via dephasing due to spin-spin effect. Although the latter spin-spin contribution is degenerate with the self-spin effect as discussed in Introduction, the I-Love-Q relation can help break the degeneracy since the spin-induced quadrupole moment can be estimated from the adiabatic tidal parameter [96, 97]. On the other hand, GW luminosity during the inspiralling is more sensitive to the tidal effects rather than spin-orbit terms [98]. In particular, the tidal contribution of the primary to the luminosity reads [5]

$$\mathcal{L}_{\text{GW}}^T = \frac{192\eta^2 x^{10} (M_* + 3M_{\text{comp}}) M_*^4 \Lambda_*}{5(M_* + M_{\text{comp}})^5}, \quad (43)$$

while the spin-orbit effects give only negligible amount to it. Therefore, by correlating the tidal imprints in the phasing and the luminosity, we may be able to determine better the tidal parameters. Nonetheless, we note that the above equation applies to non-spinning NSs.

In reality, the effect of tides in the tidal evolution and dephasing is 3-fold: *gravito-electric*, *gravito-magnetic* tides, and the *change in the waveform* shape induced from the gravito-electric tidal field [99–101]. We focus in the present article the gravito-electric tides, while we note that some excitations ignited by the gravito-

magnetic tidal field [70, 102] may become comparable to the gravito-electric excitations under certain conditions [103]. In addition, although we consider the spin-influenced tidal effects in GW phase, we do not include the spin-corrected orbital motion, and the rotation-induced deformation of NSs in the present article. Despite the minor spin contribution in the GW dephasing compared to the tidally-induced phase shift (e.g., [93]), the uncertainty in the spin contribution will deteriorate the estimation of the tidal parameters. Detailed analysis accounting for the other types of tides, and including the spin-induced dephasing would be useful in this direction. In addition, during the preparation of this article, there is an investigation [104] pointing out the importance of tidal-spin interaction in the waveform modeling if the NS

spins rapidly with $\chi \gtrsim 0.1$.

ACKNOWLEDGEMENT

KK gratefully acknowledges financial support by DFG research Grant No. 413873357. HJK is indebted to the support from Sandwich grant (JYP) No. 109-2927-I-007-503 by DAAD and MOST during early stages of this work.

DATA AVAILABILITY STATEMENT

Observational data used in this paper are quoted from the cited works. Data generated from computations are reported in the body of the paper. Additional data will be made available upon reasonable request.

-
- [1] A. G. Wiseman, *Phys. Rev. D* **46**, 1517 (1992).
 - [2] K. Kokkotas, A. Królak, and G. Tsegas, *Classical and Quantum Gravity* **11**, 1901 (1994).
 - [3] C. Cutler and E. E. Flanagan, *Phys. Rev. D* **49**, 2658 (1994), [arXiv:gr-qc/9402014](#).
 - [4] E. Poisson and C. M. Will, *Phys. Rev. D* **52**, 848 (1995), [arXiv:gr-qc/9502040](#).
 - [5] T. Hinderer, B. D. Lackey, R. N. Lang, and J. S. Read, *Phys. Rev. D* **81**, 123016 (2010), [arXiv:0911.3535 \[astro-ph.HE\]](#).
 - [6] T. Damour, A. Nagar, and L. Villain, *Phys. Rev. D* **85**, 123007 (2012), [arXiv:1203.4352 \[gr-qc\]](#).
 - [7] E. E. Flanagan and T. Hinderer, *Phys. Rev. D* **77**, 021502 (2008), [arXiv:0709.1915 \[astro-ph\]](#).
 - [8] J. Vines, E. E. Flanagan, and T. Hinderer, *Phys. Rev. D* **83**, 084051 (2011), [arXiv:1101.1673 \[gr-qc\]](#).
 - [9] J. E. Vines and E. E. Flanagan, *Phys. Rev. D* **88**, 024046 (2013), [arXiv:1009.4919 \[gr-qc\]](#).
 - [10] B. P. Abbott *et al.* (LIGO Scientific, Virgo), *Phys. Rev. Lett.* **121**, 161101 (2018), [arXiv:1805.11581 \[gr-qc\]](#).
 - [11] A. Guerra Chaves and T. Hinderer, *J. Phys. G* **46**, 123002 (2019), [arXiv:1912.01461 \[nucl-th\]](#).
 - [12] K. D. Kokkotas and G. Schaefer, *Mon. Not. Roy. Astron. Soc.* **275**, 301 (1995), [arXiv:gr-qc/9502034](#).
 - [13] T. Hinderer *et al.*, *Phys. Rev. Lett.* **116**, 181101 (2016), [arXiv:1602.00599 \[gr-qc\]](#).
 - [14] J. Steinhoff, T. Hinderer, A. Buonanno, and A. Taracchini, *Phys. Rev. D* **94**, 104028 (2016), [arXiv:1608.01907 \[gr-qc\]](#).
 - [15] P. Schmidt and T. Hinderer, *Phys. Rev. D* **100**, 021501 (2019), [arXiv:1905.00818 \[gr-qc\]](#).
 - [16] T. Dietrich, S. Bernuzzi, and W. Tichy, *Phys. Rev. D* **96**, 121501 (2017), [arXiv:1706.02969 \[gr-qc\]](#).
 - [17] A. Krolak, K. D. Kokkotas, and G. Schaefer, *Phys. Rev. D* **52**, 2089 (1995), [arXiv:gr-qc/9503013](#).
 - [18] L. Blanchet, T. Damour, B. R. Iyer, C. M. Will, and A. G. Wiseman, *Phys. Rev. Lett.* **74**, 3515 (1995), [arXiv:gr-qc/9501027](#).
 - [19] K. G. Arun, A. Buonanno, G. Faye, and E. Ochsner, *Phys. Rev. D* **79**, 104023 (2009), [Erratum: *Phys. Rev. D* **84**, 049901 (2011)], [arXiv:0810.5336 \[gr-qc\]](#).
 - [20] T. Dietrich *et al.*, *Phys. Rev. D* **99**, 024029 (2019), [arXiv:1804.02235 \[gr-qc\]](#).
 - [21] W. G. Laarakkers and E. Poisson, *Astrophys. J.* **512**, 282 (1999), [arXiv:gr-qc/9709033](#).
 - [22] E. Poisson, *Phys. Rev. D* **57**, 5287 (1998), [arXiv:gr-qc/9709032](#).
 - [23] M. Levi and J. Steinhoff, *JCAP* **12**, 003, [arXiv:1408.5762 \[gr-qc\]](#).
 - [24] M. Agathos, J. Meidam, W. Del Pozzo, T. G. F. Li, M. Tompitak, J. Veitch, S. Vitale, and C. Van Den Broeck, *Phys. Rev. D* **92**, 023012 (2015), [arXiv:1503.05405 \[gr-qc\]](#).
 - [25] J. Steinhoff, T. Hinderer, T. Dietrich, and F. Foucart, *Phys. Rev. Res.* **3**, 033129 (2021), [arXiv:2103.06100 \[gr-qc\]](#).
 - [26] A. Tsokaros, M. Ruiz, V. Paschalidis, S. L. Shapiro, and K. Uryū, *Phys. Rev. D* **100**, 024061 (2019), [arXiv:1906.00011 \[gr-qc\]](#).
 - [27] R. Dudi, T. Dietrich, A. Rashti, B. Bruegmann, J. Steinhoff, and W. Tichy, *Phys. Rev. D* **105**, 064050 (2022), [arXiv:2108.10429 \[gr-qc\]](#).
 - [28] I. Harry and T. Hinderer, *Class. Quant. Grav.* **35**, 145010 (2018), [arXiv:1801.09972 \[gr-qc\]](#).
 - [29] T. E. Riley *et al.*, *Astrophys. J. Lett.* **918**, L27 (2021), [arXiv:2105.06980 \[astro-ph.HE\]](#).
 - [30] G. Raaijmakers, S. K. Greif, K. Hebeler, T. Hinderer, S. Nissanke, A. Schwenk, T. E.

- Riley, A. L. Watts, J. M. Lattimer, and W. C. G. Ho, *Astrophys. J. Lett.* **918**, L29 (2021), [arXiv:2105.06981 \[astro-ph.HE\]](#).
- [31] D. Radice, A. Perego, F. Zappa, and S. Bernuzzi, *Astrophys. J. Lett.* **852**, L29 (2018), [arXiv:1711.03647 \[astro-ph.HE\]](#).
- [32] M. Fasano, T. Abdelsalhin, A. Maselli, and V. Ferrari, *Phys. Rev. Lett.* **123**, 141101 (2019), [arXiv:1902.05078 \[astro-ph.HE\]](#).
- [33] G. Pratten, P. Schmidt, and N. Williams, *arXiv eprint* 2109.07566 (2021).
- [34] G. Pratten, P. Schmidt, and T. Hinderer, *Nature Communications* **11**, 2553 (2020), [arXiv:1905.00817 \[gr-qc\]](#).
- [35] N. Williams, G. Pratten, and P. Schmidt, *arXiv e-prints*, [arXiv:2203.00623](#) (2022), [arXiv:2203.00623 \[astro-ph.HE\]](#).
- [36] H.-J. Kuan, A. G. Suvorov, and K. D. Kokkotas, *Mon. Not. Roy. Astron. Soc.* **506**, 2985–2998 (2021), [arXiv:2106.16123 \[gr-qc\]](#).
- [37] C. Cutler *et al.*, *Phys. Rev. Lett.* **70**, 2984 (1993), [arXiv:astro-ph/9208005](#).
- [38] B. P. Abbott *et al.* (LIGO Scientific, Virgo), *Phys. Rev. Lett.* **119**, 161101 (2017), [arXiv:1710.05832 \[gr-qc\]](#).
- [39] N.-B. Zhang and B.-A. Li, *Astrophys. J.* **902**, 38 (2020), [arXiv:2007.02513 \[astro-ph.HE\]](#).
- [40] E. R. Most, L. J. Papenfort, L. R. Weih, and L. Rezzolla, *Mon. Not. Roy. Astron. Soc.* **499**, L82 (2020), [arXiv:2006.14601 \[astro-ph.HE\]](#).
- [41] B. Biswas, R. Nandi, P. Char, S. Bose, and N. Stergioulas, *Mon. Not. Roy. Astron. Soc.* **505**, 1600 (2021), [arXiv:2010.02090 \[astro-ph.HE\]](#).
- [42] S. Droz, D. J. Knapp, E. Poisson, and B. J. Owen, *Phys. Rev. D* **59**, 124016 (1999), [arXiv:gr-qc/9901076](#).
- [43] L. Baiotti, T. Damour, B. Giacomazzo, A. Nagar, and L. Rezzolla, *Phys. Rev. D* **84**, 024017 (2011), [arXiv:1103.3874 \[gr-qc\]](#).
- [44] L. Blanchet, *Living Rev. Rel.* **17**, 2 (2014), [arXiv:1310.1528 \[gr-qc\]](#).
- [45] A. Buonanno and T. Damour, *Phys. Rev. D* **59**, 084006 (1999), [arXiv:gr-qc/9811091](#).
- [46] T. Damour and A. Nagar, *Phys. Rev. D* **79**, 081503 (2009), [arXiv:0902.0136 \[gr-qc\]](#).
- [47] T. Damour, A. Nagar, and S. Bernuzzi, *Phys. Rev. D* **87**, 084035 (2013), [arXiv:1212.4357 \[gr-qc\]](#).
- [48] K. Kawaguchi, K. Kiuchi, K. Kyutoku, Y. Sekiguchi, M. Shibata, and K. Taniguchi, *Phys. Rev. D* **97**, 044044 (2018), [arXiv:1802.06518 \[gr-qc\]](#).
- [49] T. Dietrich, A. Samajdar, S. Khan, N. K. Johnson-McDaniel, R. Dudi, and W. Tichy, *Phys. Rev. D* **100**, 044003 (2019), [arXiv:1905.06011 \[gr-qc\]](#).
- [50] M. Boyle, D. A. Brown, L. E. Kidder, A. H. Mroue, H. P. Pfeiffer, M. A. Scheel, G. B. Cook, and S. A. Teukolsky, *Phys. Rev. D* **76**, 124038 (2007), [arXiv:0710.0158 \[gr-qc\]](#).
- [51] K. Hotokezaka, K. Kyutoku, H. Okawa, and M. Shibata, *Phys. Rev. D* **91**, 064060 (2015), [arXiv:1502.03457 \[gr-qc\]](#).
- [52] S. Bernuzzi, A. Nagar, T. Dietrich, and T. Damour, *Phys. Rev. Lett.* **114**, 161103 (2015), [arXiv:1412.4553 \[gr-qc\]](#).
- [53] D. Lai, *Mon. Not. Roy. Astron. Soc.* **270**, 611 (1994), [arXiv:astro-ph/9404062](#).
- [54] T. Damour and A. Nagar, *Phys. Rev. D* **81**, 084016 (2010), [arXiv:0911.5041 \[gr-qc\]](#).
- [55] D. Bini, T. Damour, and G. Faye, *Phys. Rev. D* **85**, 124034 (2012), [arXiv:1202.3565 \[gr-qc\]](#).
- [56] B. D. Lackey, S. Bernuzzi, C. R. Galley, J. Meidam, and C. Van Den Broeck, *Phys. Rev. D* **95**, 104036 (2017), [arXiv:1610.04742 \[gr-qc\]](#).
- [57] L. E. Kidder, C. M. Will, and A. G. Wiseman, *Phys. Rev. D* **47**, R4183 (1993), [arXiv:gr-qc/9211025](#).
- [58] T. A. Apostolatos, C. Cutler, G. J. Sussman, and K. S. Thorne, *Phys. Rev. D* **49**, 6274 (1994).
- [59] M. E. Alexander, *Mon. Not. Roy. Astron. Soc.* **227**, 843 (1987).
- [60] A. Maselli, L. Gualtieri, F. Pannarale, and V. Ferrari, *Phys. Rev. D* **86**, 044032 (2012), [arXiv:1205.7006 \[gr-qc\]](#).
- [61] M. Favata, *Phys. Rev. Lett.* **112**, 101101 (2014), [arXiv:1310.8288 \[gr-qc\]](#).
- [62] L. Wade, J. D. E. Creighton, E. Ochsner, B. D. Lackey, B. F. Farr, T. B. Littenberg, and V. Raymond, *Phys. Rev. D* **89**, 103012 (2014), [arXiv:1402.5156 \[gr-qc\]](#).
- [63] Q. Henry, G. Faye, and L. Blanchet, *Phys. Rev. D* **102**, 044033 (2020), [arXiv:2005.13367 \[gr-qc\]](#).
- [64] G. Schafer, *Annals Phys.* **161**, 81 (1985).
- [65] T. Damour, P. Jaranowski, and G. Schafer, *Phys. Rev. D* **62**, 044024 (2000), [arXiv:gr-qc/9912092](#).
- [66] T. Dietrich, T. Hinderer, and A. Samajdar, *Gen. Rel. Grav.* **53**, 27 (2021), [arXiv:2004.02527 \[gr-qc\]](#).
- [67] H. M  ther, M. Prakash, and T. L. Ainsworth, *Phys. Lett. B* **199**, 469 (1987).
- [68] B. D. Lackey, M. P  rre, A. Taracchini, and S. Marsat, *Phys. Rev. D* **100**, 024002 (2019), [arXiv:1812.08643 \[gr-qc\]](#).
- [69] H.-J. Kuan, C. J. Kr  ger, A. G. Suvorov, and K. D. Kokkotas, *MNRAS* **10.1093/mnras/stac1101** (2022), [arXiv:2204.08492 \[gr-qc\]](#).
- [70] S. Ma, H. Yu, and Y. Chen, *Phys. Rev. D* **103**, 063020 (2021), [arXiv:2010.03066 \[gr-qc\]](#).
- [71] J. M. Lattimer and B. F. Schutz, *Astrophys. J.* **629**, 979 (2005), [arXiv:astro-ph/0411470](#).
- [72] C. Raithel, F.   zel, and D. Psaltis, *Astrophys. J. Lett.* **857**, L23 (2018), [arXiv:1803.07687 \[astro-ph.HE\]](#).
- [73] T. Zhao and J. M. Lattimer, *Phys. Rev. D* **98**, 063020 (2018), [arXiv:1808.02858 \[astro-ph.HE\]](#).
- [74] S. De, D. Finstad, J. M. Lattimer, D. A. Brown, E. Berger, and C. M. Biwer, *Phys. Rev. Lett.* **121**, 091102 (2018), [Erratum: *Phys. Rev. Lett.* **121**, 259902 (2018)], [arXiv:1804.08583 \[astro-ph.HE\]](#).

- [75] C. J. Krüger and K. D. Kokkotas, *Phys. Rev. Lett.* **125**, 111106 (2020), [arXiv:1910.08370 \[gr-qc\]](#).
- [76] C. J. Krüger and K. D. Kokkotas, *Phys. Rev. D* **102**, 064026 (2020), [arXiv:2008.04127 \[gr-qc\]](#).
- [77] C. J. Krüger, K. D. Kokkotas, P. Manoharan, and S. H. Völkel, *Frontiers in Astronomy and Space Sciences* **8**, 166 (2021), [arXiv:2110.00393 \[gr-qc\]](#).
- [78] M. Hannam, D. A. Brown, S. Fairhurst, C. L. Fryer, and I. W. Harry, *Astrophys. J. Lett.* **766**, L14 (2013), [arXiv:1301.5616 \[gr-qc\]](#).
- [79] P. Landry and E. Poisson, *Phys. Rev. D* **91**, 104018 (2015), [arXiv:1503.07366 \[gr-qc\]](#).
- [80] P. Pani, L. Gualtieri, A. Maselli, and V. Ferrari, *Phys. Rev. D* **92**, 024010 (2015), [arXiv:1503.07365 \[gr-qc\]](#).
- [81] M. Burgay *et al.*, *Nature* **426**, 531 (2003), [arXiv:astro-ph/0312071](#).
- [82] L. S. Finn and D. F. Chernoff, *Phys. Rev. D* **47**, 2198 (1993), [arXiv:gr-qc/9301003](#).
- [83] R. Abbott *et al.* (LIGO Scientific, Virgo), *Astrophys. J. Lett.* **896**, L44 (2020), [arXiv:2006.12611 \[astro-ph.HE\]](#).
- [84] K.-W. Lo and L.-M. Lin, *Astrophys. J.* **728**, 12 (2011), [arXiv:1011.3563 \[astro-ph.HE\]](#).
- [85] M. A. Sedda, *Commun. Phys.* **3**, 43 (2020), [arXiv:2003.02279 \[astro-ph.GA\]](#).
- [86] M. Arca Sedda, *Astrophys. J. Lett.* **908**, L38 (2021), [arXiv:2102.03364 \[astro-ph.HE\]](#).
- [87] W. Lu, P. Beniamini, and C. Bonnerot, *Mon. Not. Roy. Astron. Soc.* **500**, 1817 (2020), [arXiv:2009.10082 \[astro-ph.HE\]](#).
- [88] R. A. Mardling, in *Dynamical Evolution of Star Clusters: Confrontation of Theory and Observations*, Vol. 174, edited by P. Hut and J. Makino (1996) p. 273.
- [89] T. Yamamoto, M. Shibata, and K. Taniguchi, *Phys. Rev. D* **78**, 064054 (2008), [arXiv:0806.4007 \[gr-qc\]](#).
- [90] T. Dietrich, S. Bernuzzi, M. Ujevic, and W. Tichy, *Phys. Rev. D* **95**, 044045 (2017), [arXiv:1611.07367 \[gr-qc\]](#).
- [91] E. R. Most, L. J. Papenfort, A. Tsokaros, and L. Rezzolla, *Astrophys. J.* **884**, 40 (2019), [arXiv:1904.04220 \[astro-ph.HE\]](#).
- [92] M. Ruiz, A. Tsokaros, V. Paschalidis, and S. L. Shapiro, *Phys. Rev. D* **99**, 084032 (2019), [arXiv:1902.08636 \[astro-ph.HE\]](#).
- [93] T. Dietrich and M. Ujevic, *Class. Quant. Grav.* **34**, 105014 (2017), [arXiv:1612.03665 \[gr-qc\]](#).
- [94] W. E. East, V. Paschalidis, F. Pretorius, and A. Tsokaros, *Phys. Rev. D* **100**, 124042 (2019), [arXiv:1906.05288 \[astro-ph.HE\]](#).
- [95] H.-J. Kuan, A. G. Suvorov, and K. D. Kokkotas, submitted to MNRAS as a Letter (2022).
- [96] K. Yagi and N. Yunes, *Science* **341**, 365 (2013), [arXiv:1302.4499 \[gr-qc\]](#).
- [97] K. Yagi and N. Yunes, *Phys. Rev. D* **88**, 023009 (2013), [arXiv:1303.1528 \[gr-qc\]](#).
- [98] F. Zappa, S. Bernuzzi, D. Radice, A. Perego, and T. Dietrich, *Phys. Rev. Lett.* **120**, 111101 (2018), [arXiv:1712.04267 \[gr-qc\]](#).
- [99] T. Damour and A. Nagar, *Phys. Rev. D* **80**, 084035 (2009), [arXiv:0906.0096 \[gr-qc\]](#).
- [100] E. Poisson, *Phys. Rev. D* **101**, 104028 (2020), [arXiv:2003.10427 \[gr-qc\]](#).
- [101] E. Poisson, *Phys. Rev. D* **102**, 064059 (2020), [arXiv:2007.01678 \[gr-qc\]](#).
- [102] P. K. Gupta, J. Steinhoff, and T. Hinderer, *Phys. Rev. Res.* **3**, 013147 (2021), [arXiv:2011.03508 \[gr-qc\]](#).
- [103] E. Poisson and C. Buisson, *Phys. Rev. D* **102**, 104005 (2020), [arXiv:2007.03050 \[gr-qc\]](#).
- [104] G. Castro, L. Gualtieri, A. Maselli, and P. Pani, *arXiv e-prints*, [arXiv:2204.12510](#) (2022), [arXiv:2204.12510 \[gr-qc\]](#).